NONLINEAR MODEL IDENTIFICATION OF A MARINE PROPELLER OVER FOUR-QUADRANT OPERATIONS

Luca Pivano * **Thor Inge Fossen** *
Tor Arne Johansen *

* *Department of Engineering Cybernetics, Norwegian University of Science and Technology, N-7491 Norway*

Abstract: This paper proposes a nonlinear dynamics model for a marine propeller able to reproduce the propeller thrust over the full four-quadrant range of propeller shaft speed and vessel speed. A two-state model has been identified from experimental data. The model includes a state equation for the propeller shaft speed and one that describes the dynamics of the axial flow velocity. The model reproduces accurately propeller thrust and torque over a wide range of operation.

Keywords: Identification, marine, modeling, nonlinear, propulsion

1. INTRODUCTION

Maneuvering and dynamic positioning control of marine vessels represent a difficult design problem. Our ability to design a good control system is limited principally by the problem to understand the vessel's and the propeller's dynamics besides the problem to measure the environmental state. A better dynamics model for thruster and propellers will lead to better control performances.

Several dynamical models for marine thrusters have been presented in the last fifteen years. It has been proved that the unsteady propeller dynamics can be approximated by a finite-dimensional lumped-parameter dynamical system, see (Bachmayer *et al.*, Jan. 2000), (Healey *et al.*, 1994), (Yorger *et al.*, 1990), (Blanke *et al.*, 2000).

Healey *et al.* (1994) proposed a *two-state* nonlinear model based on the motor dynamics and thin-foil propeller hydrodynamics using sinusoidal lift and drag functions. This was done by modeling a control volume of water around the propeller as a mass-damper system. This model, with shaft speed n and axial flow velocity u_p at the propeller disc as a state variables, is able to reproduce overshoots in thrust which are typically observed in experimental data. Whitcomb and Yoerger (1995) have experimentally verified the utility of the axial flow model but they found dissimilarity between the thrust provided by the propeller and the one simulated with the Healey *et al's* model in a transient response. Bachmayer *et al.* (2000) investigated for the causes of these discrepancies and it has been found that the model using experimentally derived lift and drag curves (nonsinusoidal) reproduces more accurately experimental data than models employing sinusoidal lift and drag curves. The latter model shows high accuracy in reproducing thrust and propeller shaft speed but it has been identified from data acquired during bollard-pull condition test (zero vessel speed).

A more general model that includes the effect of the transient due to the motion of the propeller through the water, has been presented by Blanke *et al.* (2000). This model, possibly valid over a wide range of operation, has not been evaluated on experimental data.

In this paper, we propose a nonlinear dynamics model of a marine propeller identified from experimental data obtained moving the propeller through the water. A nonlinear model for the axial flow velocity through the propeller blade as been identified and it shows good accuracy. This dynamical model is a new contribution since models for the axial flow dynamics presented in

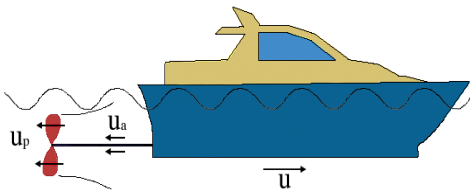

Fig. 1. Definition of axial flow velocity u_p, advance speed u_a and vessel speed u.

earlier paper have been identified only for zero vessel speed. Including the axial flow velocity dynamics in the propeller model gives better results on reproducing the measured propeller thrust and torque.

2. PROPELLER MODEL

A block diagram that represents the entire system is shown in Fig. 2. The motor generates a torque applied to the propeller shaft based on the input command.The propeller shaft speed n (or angular speed ω) is particularly influenced by the motor load, represented by the hydrodynamics torque Q_p, due to the rotation of the blades in the water. The output of the system is represented by the thrust T_p produced by the propeller.

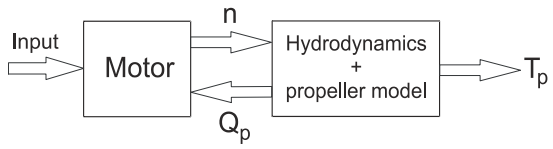

Fig. 2. System block diagram.

Fig. 1 shows a sketch of a vessel with the velocity involved. The vessel speed u is relative to the earth while the axial flow velocity u_p and the advance speed u_a are relative to the propeller disc. Only components along the longitudinal axis of the propeller are considered.

2.1 Propeller shaft model

The dynamics of a propeller shaft is commonly expressed as (Fossen, 2002):

$$J_m\dot{\omega} = Q_m - Q_p - Q_f(\omega) \tag{1}$$

where J_m is the shaft moment of inertia, Q_m the motor torque, Q_p is the propeller torque, ω is the propeller angular velocity and $Q_f(\omega)$ is the friction torque which is mainly due to the mechanical transmission. The angular shaft speed ω is considered positive when the propeller rotates in order to produce a positive vessel speed.

2.2 Hydrodynamic Model

To derive the hydrodynamic model we first considered the vessel at rest ($u = u_a = 0$) building a model for zero vessel speed (bollard-pull model). Secondly, we modified the equation obtained at the first step considering the case when the propeller moves through the water (maneuvering model) or it is subject to a current.

2.2.1. Bollard-pull model ($u_a = 0$) Considering the propeller as an infinitely thin disc of area A_0 in the mid-section of a cylinder of water of length l and mass m_f (Bernoulli tube) we can apply the momentum theory (Lewis, 1988) relating the axial thrust to the rate of change of momentum through the control volume:

$$T_p = m_f\dot{u}_p + \rho A_0 K_f |u_p| u_p \tag{2}$$

where T_P is the propeller thrust, ρ is the water density and K_f is the axial flow form factor, which has to be identified from experimental data.

Defining $d_{f_1} = \rho A_0 K_f$, the Eq. (2) governing the axial flow dynamics can be rewritten as:

$$m_f\dot{u}_p = -d_{f_1} |u_p| u_p + T_p \tag{3}$$

where the positive nonlinear damping coefficient d_{f_1} and the equivalent water inertia m_f have to be identified.

2.2.2. Maneuvering model ($u_a \neq 0$) The dynamics of the axial flow velocity is influenced by the advanced speed. Considering Fig. 3 and positive velocities, we can write the dynamics of the mass of water in the Bernoulli tube as (Blanke *et al.*, 2000):

$$m_f\dot{u}_p = T_p + \frac{1}{2}\rho A_0(u_a^2 - u_w^2) \tag{4}$$

where u_w is defined as the wake velocity.

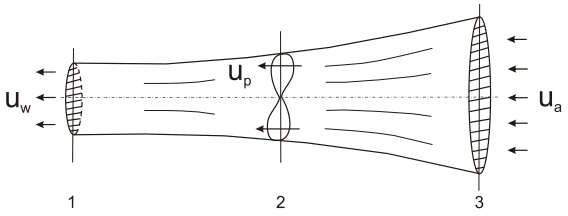

Fig. 3. Flow velocities: advance speed u_a (cross-section 3), axial flow velocity u_p at the propeller disc (cross-section 2) and wake speed u_w (cross-section 1).

When the blades rotate in order to accelerate the incoming water flow of speed u_a, the axial flow velocity u_p at the propeller disc section will be greater than u_a because the fluid acquires some speed before it reaches the disc as it results from momentum theory (Lewis, 1988). This allows us to write:

$$u_p = au_w + (1 - a)u_a \tag{5}$$

where $0 < a < 1$ is constant. Solving the Eq. (5) for u_w and substituting the expression of u_w in Eq. (4) we can derive the dynamics of the axial flow velocity at the propeller disc:

$$m_f\dot{u}_p = -d_{f_1}u_p^2 + d_{f_2}u_p u_a + d_{f_3}u_a^2 + T_p \tag{6}$$

where $d_{f_1} = \frac{1}{2a^2}\rho A_0$, $d_{f2} = \frac{1-a}{a^2}\rho A_0$ and $d_{f3} = \frac{2a-1}{2a^2}\rho A_0$.

Moreover when a propeller operates in a hull wake the propeller thrust must be multiplied by $(1-t)$ where t is the thrust deduction number and the inflow velocity u_a is obtained multiplying the vessel speed u by $(1-w)$ where w $(0 < w < 1)$ is the wake fraction number. In steady-state and forward vessel speed, w can be considered constant and positive but it can assume also small negative value for high-speed ship (Lewis, 1988).

To take into account of negative velocities and the wake fraction number, Eq. (6) must be rewritten as:

$$\begin{aligned} m_f \dot{u}_p = &-d_{f_1} |u_p| u_p + d_{f_2} |u_p| u(1-w) \\ &+d_{f_3} |u(1-w)| u(1-w) + T_p \end{aligned} \tag{7}$$

where d_{f_1}, d_{f_2}, d_{f_3} are constant and positive.

When the propeller rotates to push the water in the opposite direction with respect the direction of the inlet flow (crash-back and crash-ahead) the axial flow velocity becomes unsteady and complex (Vysohlid and Mahesh, 2004). As long the propeller rotates fast enough to reverse the inlet flow in the region close to the blades (region of reversed flow), a recirculation zone (often called a ring vortex) is observable (Vysohlid and Mahesh, 2004). This is due to the interaction between the inlet flow and the reversed flow. In this particular case the momentum theory may give more inaccurate model due to the presence of unsteady flows.

Taking the average of the measured axial flow velocity, we found that the model of Eq. (7) is still valid as long the magnitude of axial flow velocity u_p, induced by the propeller, is greater than the magnitude of the inlet water flow u_a. Vice versa, when the propeller rotates with a speed under certain values (depending on the vessel velocity), it is not able to reverse the incoming flow and the model of Eq. (7) is not accurate. The propeller behaves as a brake for the water that passes through the blades and it reduces the speed of the inlet flow. This can be represented by a second dynamical model that has been experimentally derived measuring the 3D axial flow velocity around the propeller:

$$\begin{aligned} m_f \dot{u}_p = &-d_{f_4} u_p + d_{f_5} u(1-w) \\ &+d_{f_6} |u(1-w)| u(1-w) + T_p \end{aligned} \tag{8}$$

where d_{f_4}, d_{f_5}, d_{f_6} are constant and positive.

2.3 Four-quadrant propeller thrust and torque mapping

The propeller characteristic for the four-quadrant plane composed by the shaft speed and the advance speed, is usually presented in the form of non-dimensional thrust and torque coefficients C_T and C_Q measured in steady-state conditions. Fig. 4 represents the open water characteristic relative to the propeller considered in this paper. The coefficients C_T and C_Q can be represented, for example, by a Fourier type series (Carlton, 1994) as shown in Fig. 4.

The advance angle β is computed with the four quadrant inverse tangent function as:

$$\beta = atan2\left(u_a, 0.7R\omega\right) \tag{9}$$

where R is the propeller disc radius. Thrust and torque coefficient are computed as following (Carlton, 1994):

$$C_T = \frac{T_P}{\frac{1}{2}\rho V_r^2 A_0} \tag{10}$$

$$C_Q = \frac{Q_P}{\frac{1}{2}\rho V_r^2 A_0 D} \tag{11}$$

where A_0 is the propeller disc area, D is the propeller diameter and V_r is the relative advance velocity:

$$V_r^2 = u_a^2 + (0.7R\omega)^2 \tag{12}$$

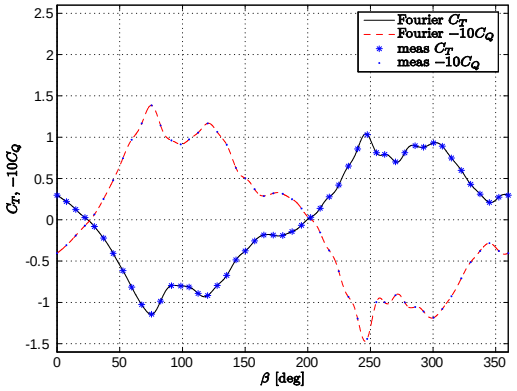

Fig. 4. Propeller four-quadrant open water characteristic.

Using this kind of characteristics we are able to reproduce thrust and torque in steady state condition while in the transient response the values computed can disagree with the real ones.

This motivated us to use the axial flow velocity dynamics to improve the accuracy of the model to reproduce the propeller thrust and torque even in the transient response. The idea is to identify the difference between the measured thrust and torque, $T_{P_{meas}}$ and $Q_{P_{meas}}$, and the ones computed with the open water characteristic, $T_{P_{OC}}$ and $Q_{P_{OC}}$:

$$T_{P_D} = T_{P_{meas}} - T_{P_{OC}} \tag{13}$$

$$Q_{P_D} = Q_{P_{meas}} - Q_{P_{OC}} \tag{14}$$

To relate T_{P_D} and Q_{P_D} to the axial flow velocity u_p, a characteristic similar to the open water one can be derived. It is possible to define the new coefficients in the following way:

$$C_{T|u_p} = \frac{T_{P_D}}{\frac{1}{2}\rho A_0 u_p |u_p|}, C_{Q|u_p} = \frac{Q_{P_D}}{\frac{1}{2}\rho A_0 u_p |u_p| D} \quad (15)$$

and compute it as a function of the angle β, defined in the Eq. (9). The new coefficients derived for the propeller considered in this paper are shown in Fig. 9.

3. EXPERIMENTAL SETUP

The tests were performed at the MCLab (http://www.itk.ntnu.no/marinkyb/MCLab/), an experimental laboratory for testing scale models of ships, rigs, underwater vehicles and propulsion system, located at NTNU (Trondheim, Norway). The basin, 30m long, is equipped with a towing carriage that can reach the maximum speed of 2m/s.

Table 1. Propeller characteristics: diameter D, number of blades Z, pitch ratio P/D at $0.7R$ and expanded blade area ratio A_e/A_0

Serial number	D	Z	P/D	A_e/A_0
P1020	25cm	4	1	0.55

The thruster we have been working on employs a three-phase brushless motor driven by an input voltage and operating in torque control mode. A propeller without duct and with characteristic given in Table 1 was attached to a shaft equipped with thrust and torque sensors inside an underwater housing. The rig with motor, underwater housing, shaft and propeller was attached to the towing carriage in order to move it through the water. A Sontek 10 MHz 3D Acoustic Doppler Velocimeter (ADV) was employed to measure the flow velocity over a sampling volume of $0.25cm^3$. It was vertically mounted $7cm$ downstream the propeller with the probe x axis aligned to the propeller axis of symmetry. The distance between the sampling volume and the center of the propeller shaft was set equal to $0.7R$, where R is the radius of the propeller disc. The motor torque was controlled by a PC on board the towing carriage. Table 2 contains the list of the recorded signals with the respective sampling frequency. A sketch of the setup is shown in Fig. 5.

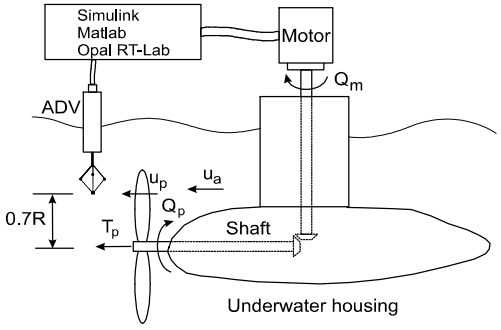

Fig. 5. Sketch of the experimental setup.

Table 2. Signals logged

Signal	f_c	Description
Q_m $[Nm]$	$200Hz$	Motor torque
Q_p $[Nm]$	$200Hz$	Propeller torque
T_p $[N]$	$200Hz$	Propeller thrust
u_p $[m/s]$	$25Hz$	Axial flow velocity
p_c $[m]$	$200Hz$	Towing carriage position
ω $[rad/s]$	$200Hz$	Propeller shaft speed

4. SYSTEM IDENTIFICATION PROCEDURE

4.1 Propeller shaft model

Referring to Eq. (1) that governs the shaft dynamics, to identify the friction curve, we ran some tests with constant motor torque. We measured the propeller angular speed and the propeller torque in steady-state condition keeping the towing carriage at rest. We derived the curve showed in Fig. 6 where we can note the presence of a static friction, a Coulomb friction and nonlinear viscous friction.

The shaft inertia has been identified using the least squares method applied to Eq. (1), once the friction curve has been derived.

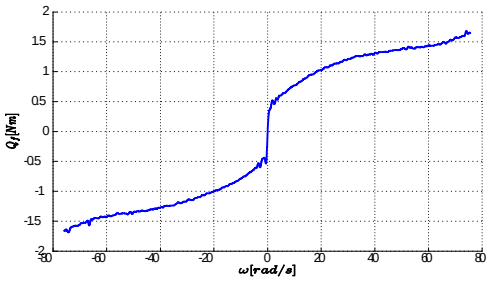

Fig. 6. Measured friction curve.

4.2 Hydrodynamic model

4.2.1. Bollard-pull model To identify the parameters present in Eq. (3) we considered first a steady-state condition. Applying steps of motor torque of different amplitudes, we measured the steady-state values of the axial flow velocity. We obtained the curve shown in Fig. 7 that proves the quadratic dependence of the propeller thrust with respect to u_p.

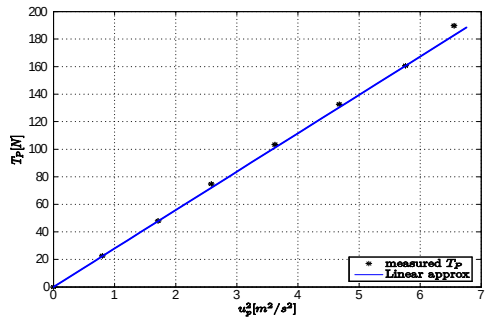

Fig. 7. Relation between axial flow velocity and propeller thrust for zero advanced speed.

The plot is relative to positive values of thrust and velocity since the probe to measure the flow speed was placed downstream the propeller We have assumed that Eq. (3) is valid also for negative u_p. The value of d_{f_1} has been estimated using the least squares method applied to the steady-state characteristic of Fig. 7 (see Table 3).

To identify the value of m_f the least squares method has been applied to the Eq. (3).

4.2.2. Maneuvering model To identify the parameters of Eq. (7) and (8) we considered the fact that in our setup, the housing that contains gear and measurement devices does not create a significant wake. The inflow velocity that has been measured is practically equal to the towing carriage speed. The wake fraction number w will be thus considered zero:

$$m_f \dot{u}_p = \begin{cases} -d_{f_4} u_p + d_{f_5} u \\ +d_{f_6} |u| u + T_p \end{cases} \text{if } \begin{matrix} \text{sgn}(u_a) = -\text{sgn}(\omega), \\ |u_p| < |u_a| \end{matrix}$$
$$\begin{cases} -d_{f_1} |u_p| u_p + d_{f_2} |u_p| u \\ +d_{f_3} |u| u + T_p \end{cases} \text{else} \quad (16)$$

Performing tests with different velocity profiles of the towing carriage and motor torque we estimated the coefficients df_2, df_3, df_4, df_5, df_6 to fit the steady-state values of the measured propeller thrust using a least squares method. The values we obtained are shown in Table 3.

4.2.3. Four-quadrant propeller thrust and torque mapping To derive the four-quadrant open water characteristic shown in Fig. 4, we performed some tests with different constant towing carriage speeds and with different constant shaft speeds. To have the desired value of ω, the shaft speed controller built-in in the motor has been used. The scheme to derive $C_{T|u_p}$ and $C_{Q|u_p}$ is presented in Fig. 8. We generated T_{OC} and Q_{OC} for several motor torque and advanced speed using the open water characteristic of Fig. 4. At the same time the model of Eq. (16) has been simulated to obtain u_p.

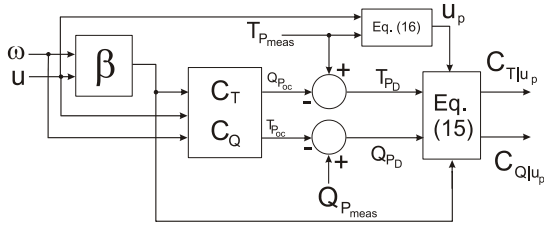

Fig. 8. Identification scheme for $C_{T|u_p}$ and $C_{Q|u_p}$.

The $C_{T|u_p}$ and $C_{Q|u_p}$ coefficients has been identified plotting the values obtained with the Eq. (15) as a function of the advanced angle β. The graphs that have been obtained had data quite scattered but it was possible to deduce the trend which is plotted in Fig. 9.

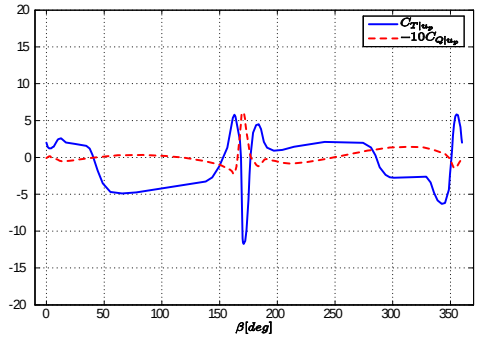

Fig. 9. Experimentally derived $C_{T|u_p}$ and $C_{Q|u_p}$.

5. EXPERIMENTAL VALIDATION

5.1 Hydrodynamics model

The model of Eq. (16), driven by the measured propeller thrust, has been simulated with different motor torque. The identified parameters are shown in Table 3. This simulation has been carried out with data that have not been used for the model identification. The results relative to two different simulations are depicted in Fig. 10 and 11.

Table 3. hydrodynamics model: experimentally identified parameters

Parameter	Value	Parameter	Value
J_m $[kgm^2]$	0.003	d_{f_3} $[kg/m]$	18.37
m_f $[kg]$	8.62	d_{f_4} $[kg/m]$	41.13
d_{f_1} $[kg/m]$	27.89	d_{f_5} $[kg/m]$	20.39
d_{f_2} $[kg/m]$	7.66	d_{f_6} $[kg/m]$	39.39

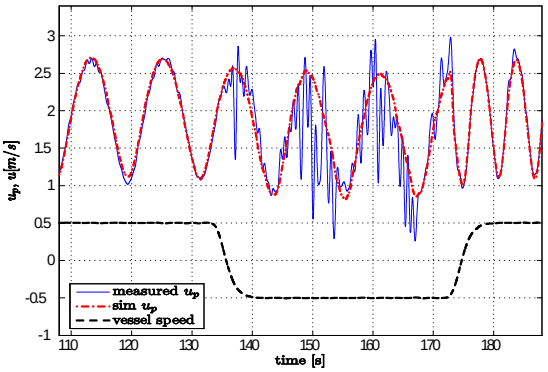

Fig. 10. Axial flow model simulation with sinusoidal motor torque and trapezoidal carriage speed.

The axial flow velocity model reproduces the measured u_p quite accurately despite the presence of noisy measurements especially when the axial flow velocity and the advance speed have opposite signs.

5.2 Overall propeller model

The overall propeller model, described by the block diagram shown in Fig. 12, has been simulated with several motor torque and several carriage speed profiles.

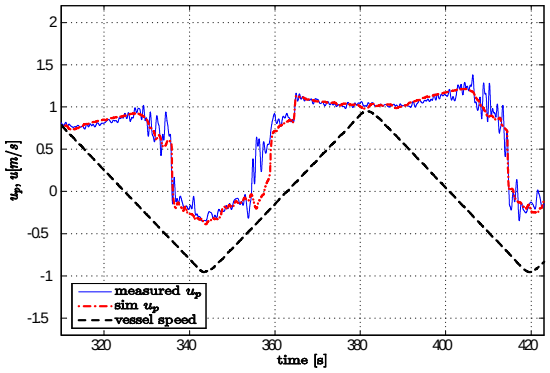

Fig. 11. Axial flow model simulation with square motor torque and triangular carriage speed.

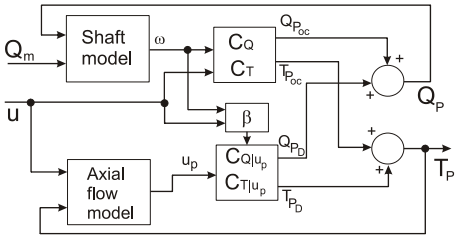

Fig. 12. Overall propeller model.

Fig. 13 and 14 show the simulated propeller thrust and torque. The model including the axial flow dynamics shows better overall accuracy in reproducing the measured propeller thrust. The model has been tested over a large number of different input motor torques: triangular, square and sinusoidal waves with various amplitudes and frequencies and with different carriage speed profiles. In all cases the model reproduced quite well the measurements.

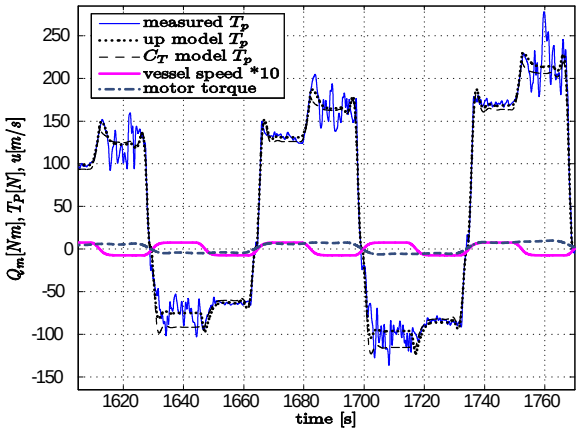

Fig. 13. Simulated propeller thrust with square motor torque.

6. CONCLUSIONS

In this paper a propeller model has been identified from data acquired in an experimental laboratory. The model is derived incorporating the dynamics of the axial flow velocity that has been identified measuring the 3D water flow around the propeller and shows good accuracy on reproducing the measurements. The flow measurement device

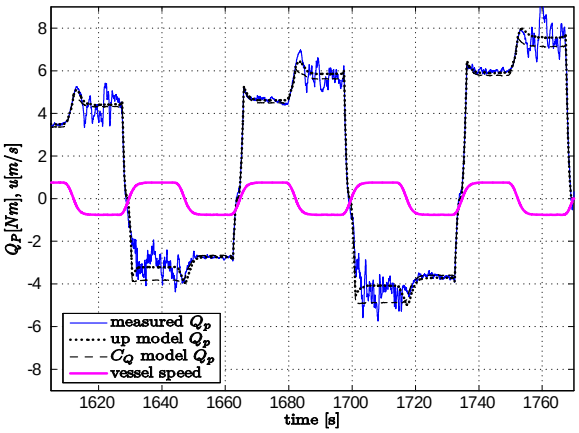

Fig. 14. Simulated propeller torque with square wave motor torque.

may be too expensive and fragile for the marine environment. To solve this problem, a nonlinear observer could be employed in order to estimate the axial flow velocity.

7. ACKNOWLEDGMENT

The authors acknowledge Øyvind N. Smogeli for valuable suggestions and discussions.

REFERENCES

Bachmayer, R., L. L.Whitcomb and M. A. Grosenbaugh (Jan. 2000). An accurate four-quadrant nonlinear dynamical model for marine thrusters: Theory and experimental validation. *IEEE J. Oceanic Eng.* **25**, 146–159.

Blanke, M., K. Lindegaard and T. I. Fossen (2000). Dynamic model for thrust generation of marine propellers. *5th IFAC Conference of Manoeuvring and Control of Marine craft, MCMC* pp. 363–368.

Carlton, J. S. (1994). *Marine Propellers and Propulsion*. Oxford, U.K.: Butterworth-Heinemann Ltd.

Fossen, T. I. (2002). *Marine Control System - Guidance, Navigation, and Control of Ships, Rigs and Underwater Vehicles*. Marine Cybernetics.

Healey, A. J., S. M. Rock, S. Cody, D. Miles and J. P. Brown (1994). Toward an improved understanding of thruster dynamics for underwater vehicles. *Symp. Autonomous Underwater Vehicle Technology, Boston MA* pp. 340–352.

Lewis, E. V. (1988). *Principles of Naval Architecture Vol II: Resistance, Propulsion and Vibration*. 3rd ed.. Society of Naval Architects and Marine Engineers. New York.

Vysohlid, M. and K. Mahesh (2004). Large-Eddy Simulation of Propeller Crashback. *APS Meeting Abstracts*.

Yorger, D. R., J. G. Cooke and J. J. E. Slotine (1990). The influence of thruster dynamics on underwater vehicles behavior and their incorporation into control system design. *IEEE Oceanic Eng.* **15**, 167–178.